Electronic Supplementary Material (ESI) for Journal of Materials Chemistry A.
This journal is © The Royal Society of Chemistry 2022

Supplementary Information

Efficient water oxidation using an Fe-doped nickel telluride–nickel phosphide electrocatalyst by partial phosphating

Yu-Jia Tang,* Yan Zou, Dongdong Zhu*

School of Chemistry and Materials Science, Institute of Advanced Materials and Flexible Electronics (IAMFE), Nanjing University of Information Science and Technology, 219 Ningliu Road, Nanjing, 210044, China
E-mail: dd.zhu@nuist.edu.cn; tangyujia@nuist.edu.cn

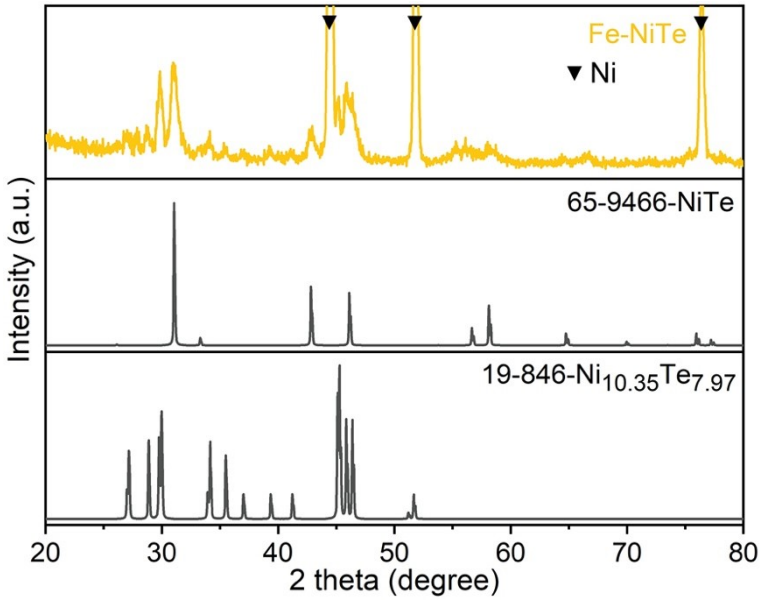

Figure S1. XRD pattern of Fe-NiTe on NF and simulated patterns of NiTe and $Ni_{10.35}Te_{7.97}$.

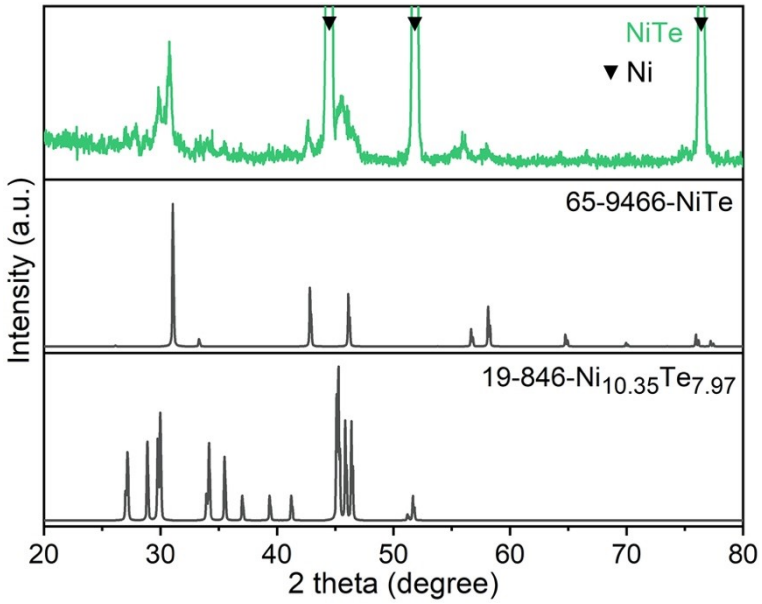

Figure S2. XRD pattern of NiTe on NF and simulated patterns of NiTe and $Ni_{10.35}Te_{7.97}$.

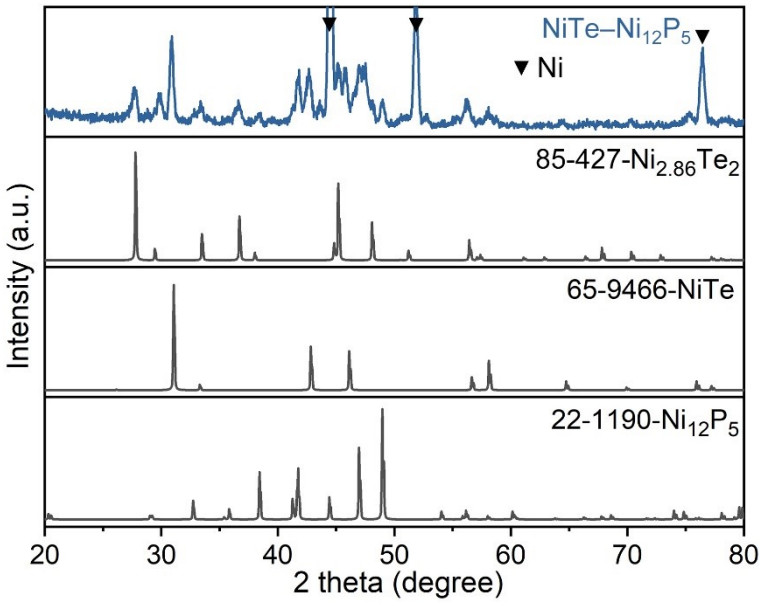

Figure S3. XRD pattern of NiTe–$Ni_{12}P_5$ on NF and simulated patterns of $Ni_{12}P_5$, NiTe and $Ni_{2.86}Te_2$.

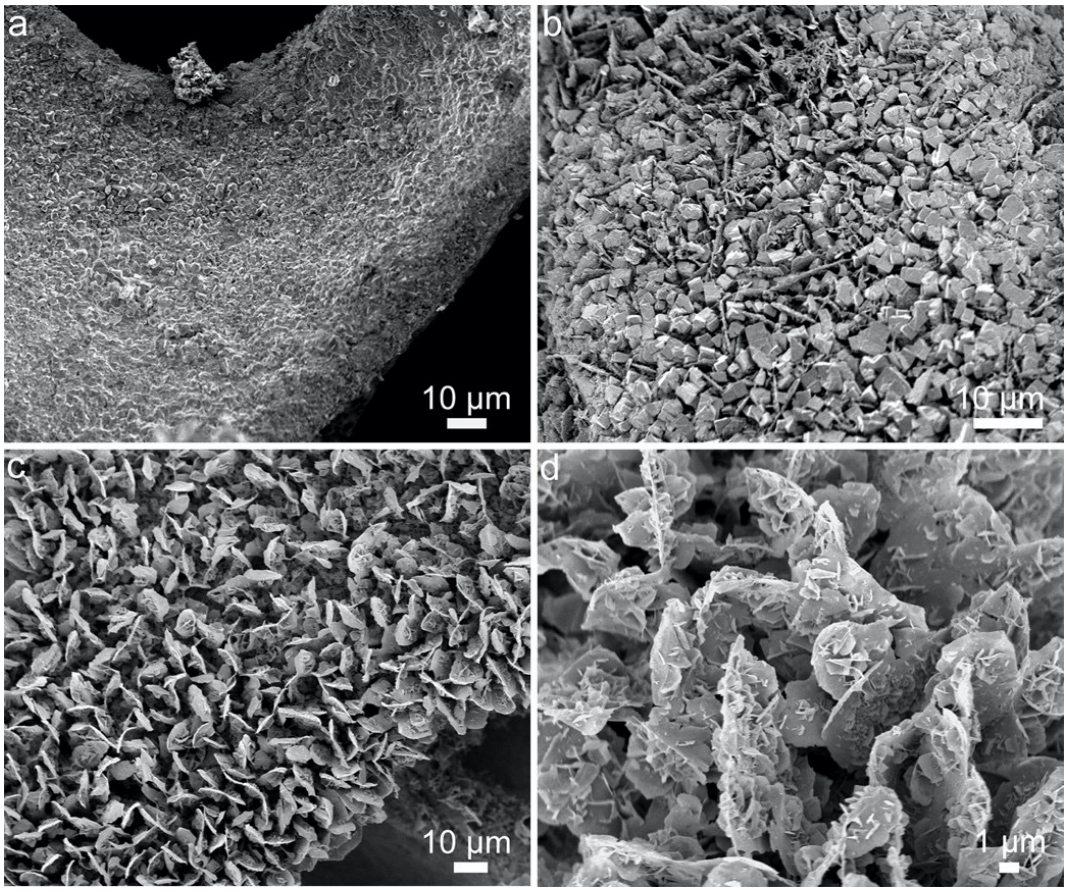

Figure S4. SEM images of (a, b) NiTe–$Ni_{12}P_5$ and (c, d) NiTe grown on the NF substrate.

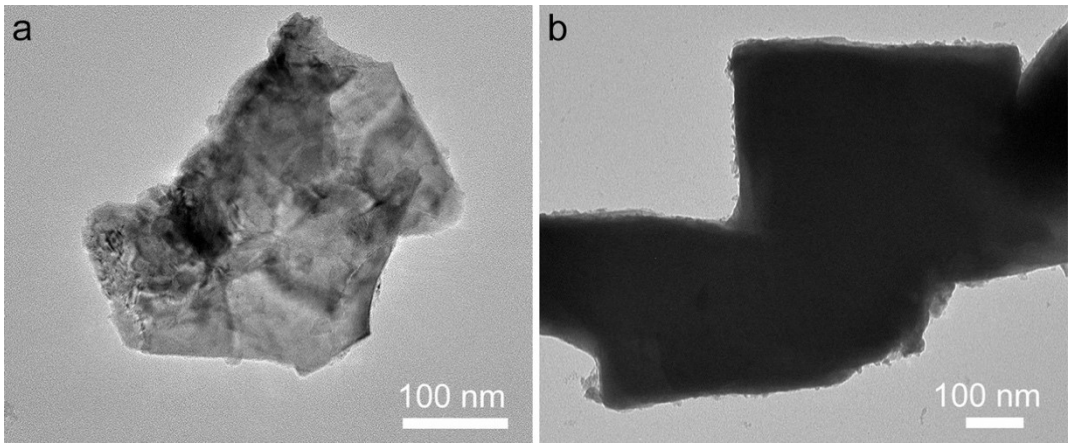

Figure S5. TEM images of Fe-NiTe–$Ni_{12}P_5$ ultrasonicated from NF.

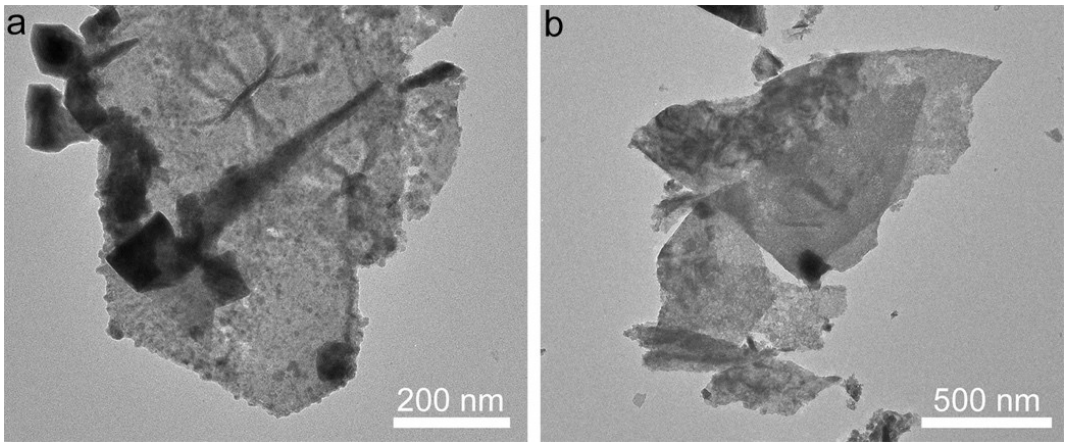

Figure S6. TEM images of (a, b) NiTe–$Ni_{12}P_5$ and (c, d) NiTe ultrasonicated from the NF substrate.

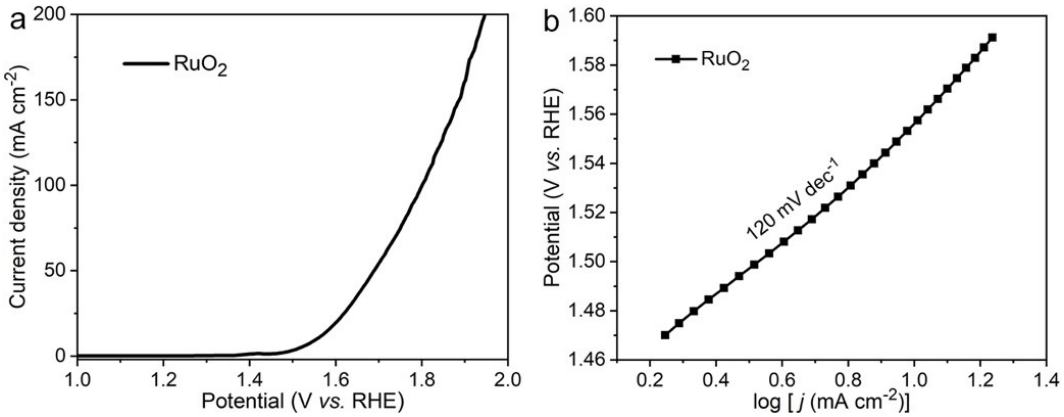

Figure S7. Electrocatalytic OER activity of the commercial RuO_2 catalyst measured in the KOH electrolyte: (a) LSV curve and (b) Tafel plot.

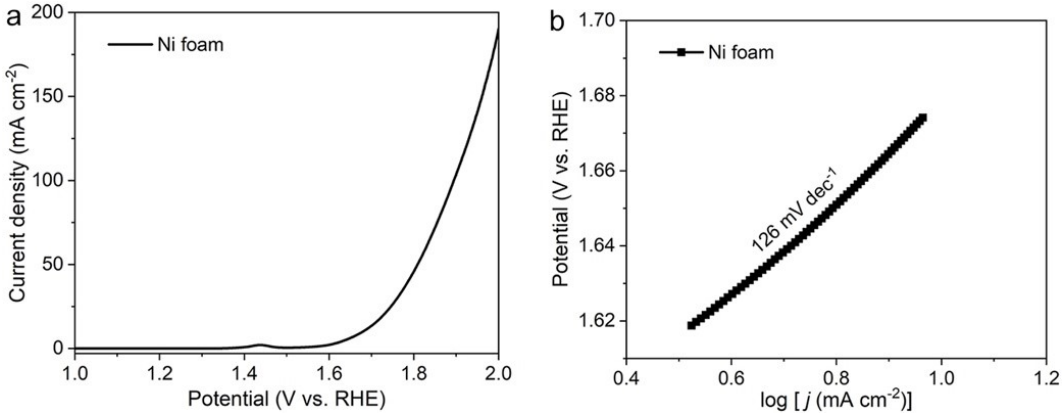

Figure S8. Electrocatalytic OER activity of NF measured in the KOH electrolyte: (a) LSV curve and (b) Tafel plot.

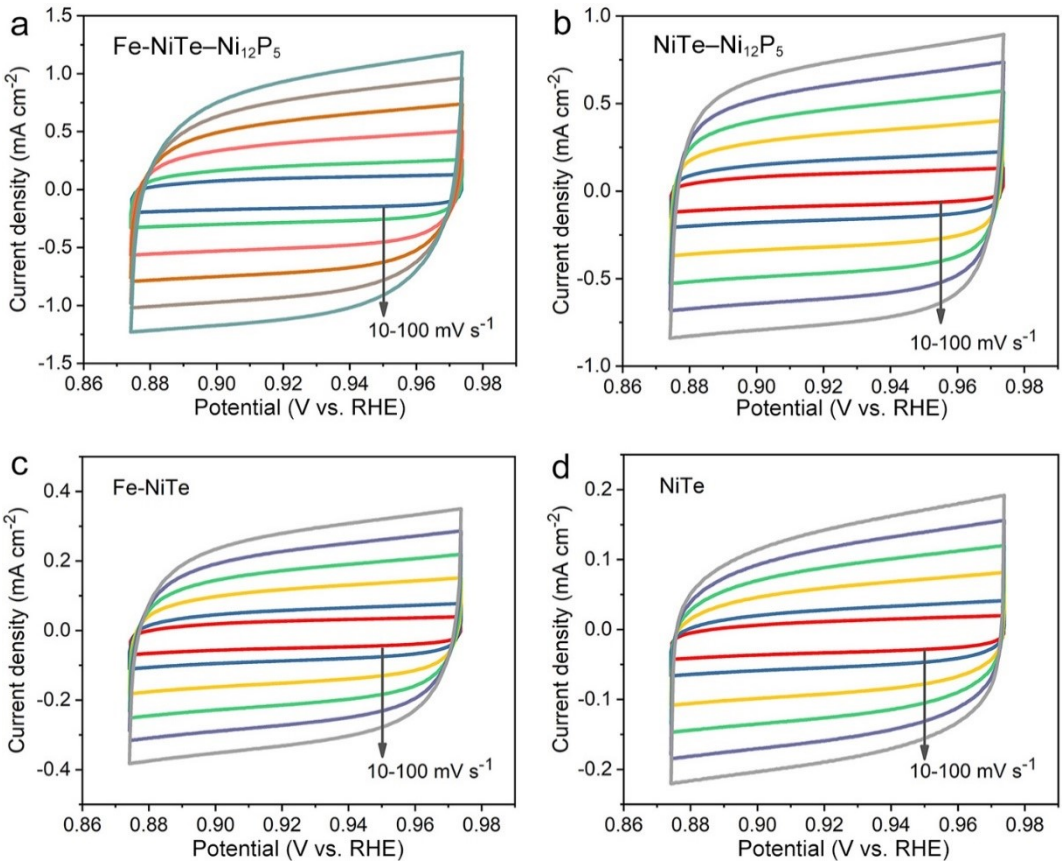

Figure S9. CV curves measured at a potential range of 0.874–0.974 V *vs.* RHE at different scan rates (10, 20, 40, 60, 80 and 100 mV s^{-1}) of (a) Fe-NiTe–$Ni_{12}P_5$, (b) NiTe–$Ni_{12}P_5$, (c) Fe-NiTe and (d) NiTe.

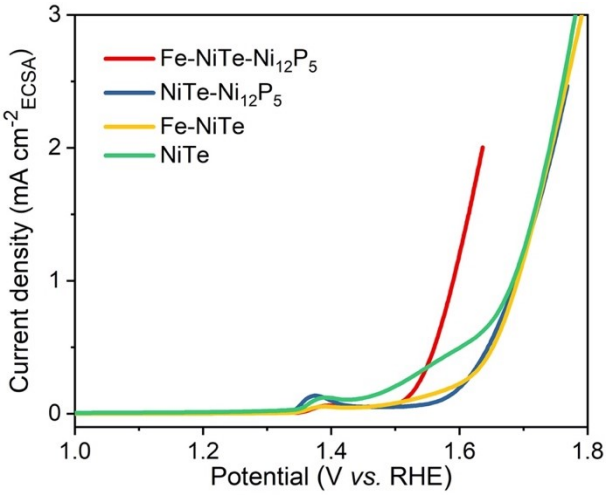

Figure S10. ECSA-normalized LSV curves of Fe-NiTe–$Ni_{12}P_5$, NiTe–$Ni_{12}P_5$, Fe-NiTe and NiTe.

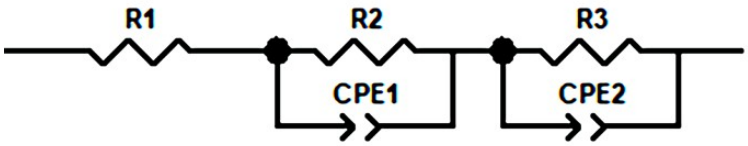

Figure S11. The equivalent circuit diagram used for EIS fitting.

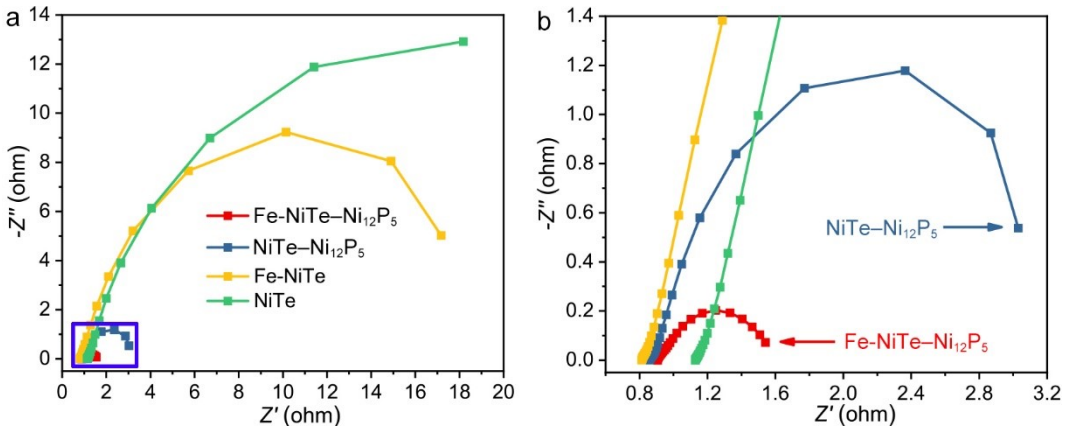

Figure S12. (a) EIS of four samples including Fe-NiTe–$Ni_{12}P_5$, NiTe–$Ni_{12}P_5$, Fe-NiTe and NiTe measured at the overpotential of 300 mV in an alkaline medium. (b) The magnified plot of the marked region of (a) in blue.

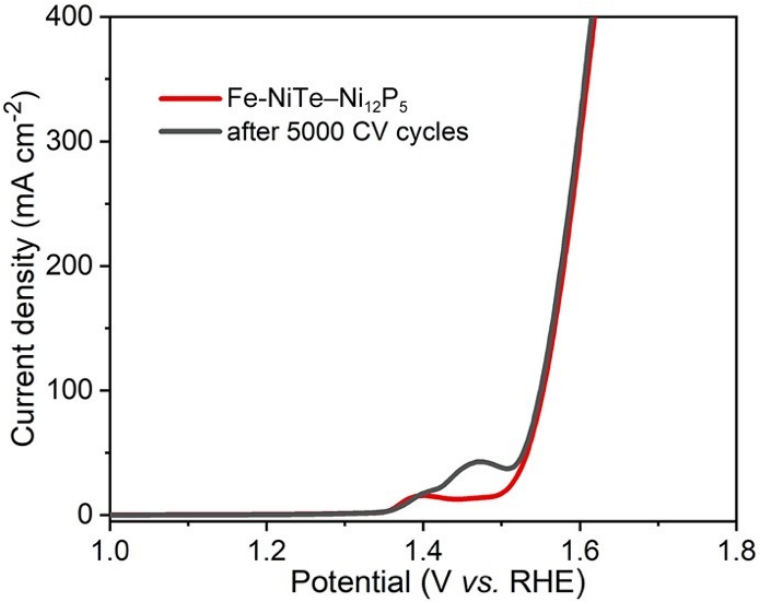

Figure S13. LSV curves of Fe-NiTe–$Ni_{12}P_5$ before and after 5000 CV cycles stability test in 1.0 M KOH.

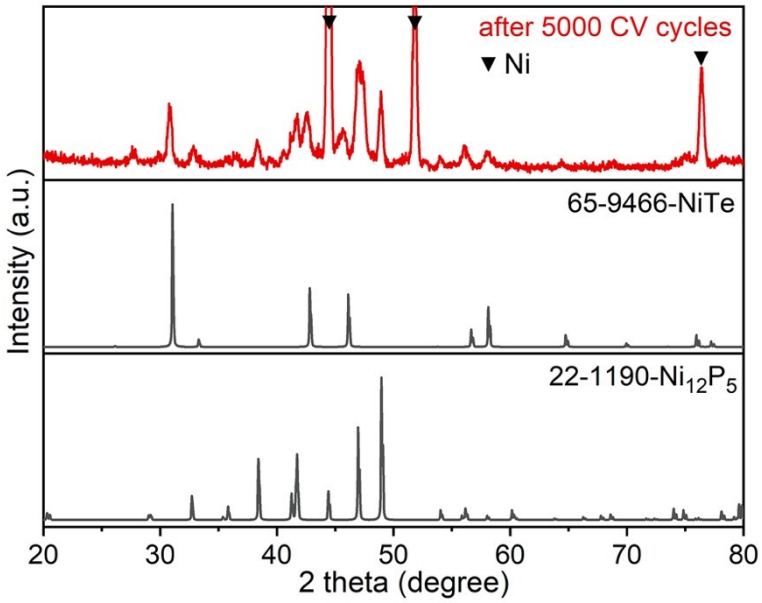

Figure S14. XRD pattern of Fe-NiTe–$Ni_{12}P_5$ on NF after the 5000 CV cycles stability test and simulated patterns of NiTe and $Ni_{12}P_5$.

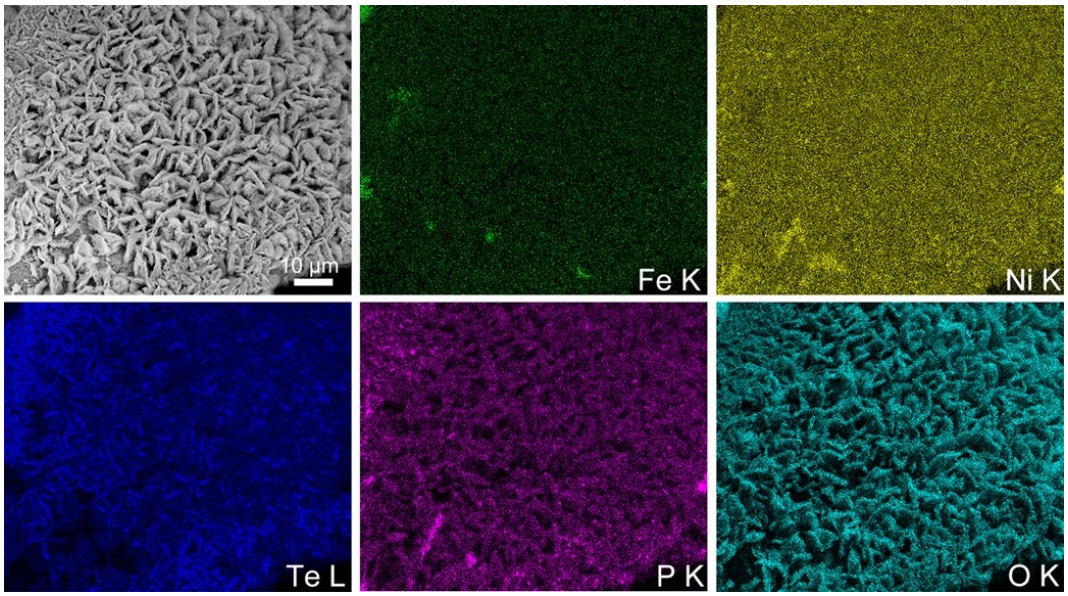

Figure S15. Elemental mapping images of Fe-NiTe–$Ni_{12}P_5$ on NF after the 5000 CV cycles stability test.

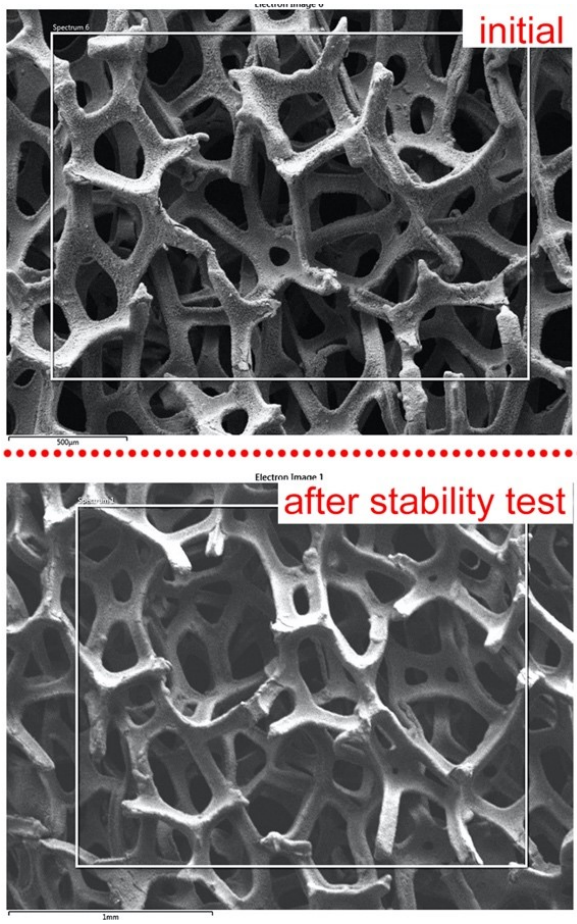

element	atomic %
Fe	1.36
Ni	59.51
Te	10.03
P	13.72
O	15.38
Total	100

element	atomic %
Fe	0.70
Ni	47.47
Te	7.63
P	8.13
O	35.31
K	0.76
Total	100

Figure S16. Atomic percentage of corresponding elements of Fe-NiTe–$Ni_{12}P_5$ on NF before and after stability test for OER by EDX analysis.

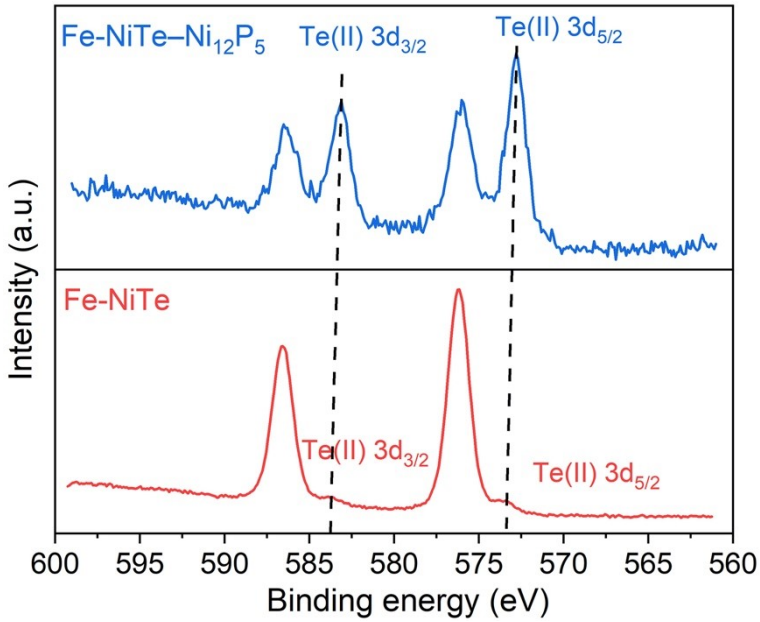

Figure S17. Te 3d XPS spectra of Fe-NiTe and Fe-NiTe–$Ni_{12}P_5$.

As can be seen in **Fig. S17**, the peaks at 583.6 and 573.3 eV correspond to Te (II) $3d_{3/2}$ and Te (II) $3d_{5/2}$ of Fe-NiTe, respectively, which are negatively shifted by around 0.5 eV after partial phosphating treatment. Such significant peak shift indicates the strong electronic interaction between NiTe and $Ni_{12}P_5$, thus optimizing the electronic structures of Fe-NiTe–$Ni_{12}P_5$.

Table S1. Atomic percentage of corresponding elements of Fe-NiTe–$Ni_{12}P_5$ on NF by XPS analysis.

	P 2p	C 1s	O 1s	Te 3d	Fe 2p	Ni 2p
Atomic %	17.35	18.92	50.04	2.17	2.39	9.14

Table S2. Comparison of electrocatalytic activities for OER of the Fe-NiTe–$Ni_{12}P_5$ catalyst and recently reported telluride-based composites.

Catalyst	Substrate	Electrolyte	η (mV) at specified current density (mA cm^{-2})		Tafel slope (mV dec^{-1})	Reference
Fe-NiTe–$Ni_{12}P_5$	Ni foam	1 M KOH	275	20	66	This work
			303	50		
			340	100		
$CoTe_2$	RRDE[a]	1 M KOH	323	10	85.1	1
$CoTe_2$	GCE[b]	0.1 M KOH	357	10	32	2
Te-Co-O	GCE	1 M KOH	380	10	58	3
$CoTe_2$-$MnTe_2$	Ti mesh	1 M KOH	310	50	118	4
$CoTe_2$@NCNTFs	GCE	1 M KOH	330	10	82.8	5
NiFe LDH/NiTe	Ni foam	1 M KOH	228	50	51.04	6
NiTe			350	50	109.09	
$CoTe_2$	Ti mesh	1 M KOH	340	50	67	7
$NiTe/NiTe_2$	Graphite rod electrode	1 M KOH	679	10	151	8
$NiTe_2$	Ti mesh	1 M KOH	315	10	82	9
NiTe-NiS	Ni foam	1 M KOH	209	10	49	10
			257	100		
Fe-NiTe-2	GCE	1 M KOH	280	10	40	11
CoTeNR	Ni foam	1 M KOH	350	100	75	12
			330	50		
NiTeNR			430	100	122	
Fe-doped Ni_2P	GCE	1 M KOH	292	10	50	13
$Ni_2P/Fe_2P/Fe_3O_4$	RDE	1 M KOH	365	10	59	14
$Ni_{0.6}Co_{1.4}P$	RDE	1 M KOH	300	10	80	15

NiFeP@NPC	RRDE	1 M KOH	350	10	78	[16]
Ni_1Co_3-P@CSs	RDE	1 M KOH	330	20	113	[17]
FeNiP/NPCS	GCE	1 M KOH	318	10	95	[18]
			470	100		

Note: [a] rotating ring–disk electrode, [b] glassy carbon electrode.

Table S3. EIS fitting data of Fe-NiTe–$Ni_{12}P_5$ and control samples for OER using a Zview2 software. R3 represents charge transfer resistance (R_{ct}).

	Fe-NiTe–$Ni_{12}P_5$	NiTe–$Ni_{12}P_5$	Fe-NiTe	NiTe
R1	0.91	0.86	0.82	1.12
R2	0.04	0.32	3.80	1.08
CPE1-T	0.12	1.33	0.62	1.92
CPE1-P	0.79	0.52	0.65	0.43
R3	**0.62**	**2.16**	**15.09**	**28.38**
CPE2-T	0.34	0.36	0.37	0.39
CPE2-P	0.74	1.00	1.03	0.92

Reference

1. T.-H. Lu, C.-J. Chen, Y.-R. Lu, C.-L. Dong and R.-S. Liu, *J. Phys. Chem. C*, 2016, **120**, 28093-28099.
2. Q. Gao, C.-Q. Huang, Y.-M. Ju, M.-R. Gao, J.-W. Liu, D. An, C.-H. Cui, Y.-R. Zheng, W.-X. Li and S.-H. Yu, *Angew. Chem. Int. Ed.*, 2017, **56**, 7769-7773.
3. I. G. McKendry, A. C. Thenuwara, J. Sun, H. Peng, J. P. Perdew, D. R. Strongin and M. J. Zdilla, *ACS Catal.*, 2016, **6**, 7393-7397.
4. Z. Wang, X. Ren, L. Wang, G. Cui, H. Wang and X. Sun, *Chem. Commun.*, 2018, **54**, 10993-10996.
5. X. Wang, X. Huang, W. Gao, Y. Tang, P. Jiang, K. Lan, R. Yang, B. Wang and R. Li, *J. Mater. Chem. A*, 2018, **6**, 3684-3691.
6. L. Hu, X. Zeng, X. Wei, H. Wang, Y. Wu, W. Gu, L. Shi and C. Zhu, *Appl. Catal., B*, 2020, **273**, 119014.
7. L. Ji, Z. Wang, H. Wang, X. Shi, A. M. Asiri and X. Sun, *ACS Sustainable Chem. Eng.*, 2018, **6**, 4481-4485.
8. K. S. Bhat, H. C. Barshilia and H. S. Nagaraja, *Int. J. Hydrogen Energy*, 2017, **42**, 24645-24655.
9. Z. Wang and L. Zhang, *ChemElectroChem*, 2018, **5**, 1153-1158.

10. Z. Xue, X. Li, Q. Liu, M. Cai, K. Liu, M. Liu, Z. Ke, X. Liu and G. Li, *Adv. Mater.*, 2019, **31**, 1900430.
11. L. Zhong, Y. Bao, X. Yu and L. Feng, *Chem. Commun.*, 2019, **55**, 9347-9350.
12. L. Yang, H. Xu, H. Liu, D. Cheng and D. Cao, *Small Methods*, 2019, **3**, 1900113.
13. G. Liu, D. He, R. Yao, Y. Zhao and J. Li, *Electrochim. Acta*, 2017, **253**, 498-505.
14. X. Peng, X. Chen, T. Liu, C. Lu, M. Sun, F. Ding, Y. Wang, P. Zou, X. Wang, Q. Zhao and H. Rao, *Chem. Asian J.*, 2019, **14**, 2744-2750.
15. B. Qiu, L. Cai, Y. Wang, Z. Lin, Y. Zuo, M. Wang and Y. Chai, *Adv. Funct. Mater.*, 2018, **28**, 1706008.
16. J. Wang and F. Ciucci, *Appl. Catal., B*, 2019, **254**, 292-299.
17. V. H. Hoa, D. T. Tran, H. T. Le, N. H. Kim and J. H. Lee, *Appl. Catal., B*, 2019, **253**, 235-245.
18. Y. Li, X. Tan, H. Tan, H. Ren, S. Chen, W. Yang, S. C. Smith and C. Zhao, *Energy Environ. Sci.*, 2020, **13**, 1799-1807.